Prediction of Subcooled Wall Boiling in a Heated Annulus Including Conjugate Heat Transfer in the Central Heated Rod

Th. Frank*, P. Beckstein*, C. Lifante*, A.D. Burns†

* ANSYS Germany GmbH, Staudenfeldweg 12, Otterfing, D-83624, Germany
† School of Process Material and Environmental Engineering, CFD Centre, University of Leeds, LS2 9JT, UK

E-mail: Thomas.Frank@ansys.com

Keywords: CFD, water-steam flow, subcooled boiling, wall boiling, CHT, phase change

Abstract

The aim of this paper is to present the validation of a newly implemented wall boiling model for the prediction of subcooled nucleate boiling under pressurized and normal conditions, so e.g. in rod bundles and fuel assemblies of PWR and BWR, first made available with full GUI support in ANSYS CFX 12.0 (ANSYS Inc., 2009). The model formulation is based on the so-called RPI wall boiling model published by Kurul & Podowski (1991) but has been extended in ANSYS 12.0 by a special approach regarding the prediction of the liquid subcooling temperature in order to make the model grid independent in the context of a CFD simulation. Furthermore the wall boiling heat partitioning algorithm has been coupled to the prediction of conjugate heat transfer in the solid material of the heated boundary of the fluid domain, allowing for the definition of volumetric energy sources in e.g. the rods of nuclear fuel assemblies heated by nuclear fission reaction. The Paper discusses the theory of the implemented model as well as the application of the model to boiling flow in vertically directed circular annulus with a centralized heated rod, as investigated by Lee et al. (2008). CFD results are compared to experiments of Lee et al. applying a hierarchy of consistently refined meshes and different CFD setup configurations including the prediction of heat transfer in the solid material of the heated rod by CHT and by prescribing a volumetric thermal energy release in the solid material instead of a prescribed wall heat flux or wall temperature at the heated boundary of the fluid flow domain.

1. Introduction

Subcooled flow boiling occurs in many industrial applications and is characterized by large heat transfer coefficients. In particular the regime of subcooled flow boiling is of interest for flows through nuclear reactor fuel assemblies of PWR and BWR. However, this efficient heat transfer mechanism is limited by the critical heat flux where the heat transfer coefficient decreases leading to a rapid heater temperature excursion potentially leading to heater melting and destruction. Therefore the occurrence of the critical heat flux flow regime has to be safely avoided. Furthermore the flow in the regime of nucleate subcooled boiling and the transition to critical heat flux is affected by many flow parameters and can be influenced by the geometrical design of the fuel assemblies. Multiphase flow morphology and bubble/slug dynamics play an important role in the radial fluid temperature and vapour distribution, substantially influencing the boiling process. From the point of view of geometry design especially the spacer grids equipped with mixing vanes are of importance in increasing the permissible heat flux.

The study of fuel assembly designs and factors of influence on the boiling process usually requires extraordinary expensive experiments. Therefore the supplementation or even the replacement of experiments by numerical analyses are of relevant interest in the study of boiling flows. Since flow patterns in boiling flows in e.g. fuel assemblies are complex 3d with lateral crossflows and resulting steam redistribution on heater surfaces, it is highly desirable to derive CFD methods for the accurate prediction of boiling processes. The paper describes the actual implementation of a wall boiling model in ANSYS CFX 12.0 and its application to a validation testcase under normal pressure conditions similar to conditions in fuel assemblies of BWR. Special attention has been given to the raise of the constant wall heat flux assumption by facilitating the coupled heat transfer prediction in adjacent solid and fluid domains of the flow configuration for wall boiling processes and thereby predicting the wall heat flux directly.

2. Nomenclature

a	bubble influence factor
A_1	wall fraction cooled by single-phase convection
A_2	wall fraction cooled by quenching
A_{LG}	interfacial area density
C_{pL}	specific heat capacity of liquid
C_{pG}	specific heat capacity of vapour
d_B	bubble diameter in the bulk flow
d_W	bubble departure diameter on the wall
f	bubble departure frequency
g	gravitational acceleration
G	mass flow rate
h_{LG}	interfacial heat transfer coefficient
H_{LG}	evaporation enthalpy
h_Q	coefficient for heat transfer by quenching
k_L	liquid heat conductivity

L_M	height of the measurement cross section
L_T	length of the experimental test section
N_a	active nucleation site density
Nu	Nusselt number
Pr	Prandtl number of liquid
q´´	wall heat flux
Q_C	heat flux due to single-phase convection
Q_E	heat flux due to evaporation
Q_Q	heat flux due to quenching
Q_W	total wall heat flux
r	radius
R	inner radius of outer tube
R_0	outer radius of inner tube/heating rod
R_P	dimensionless width of the circular annulus
Re	Reynolds number
r_G	Volume fraction of gaseous phase
T_L	near-wall liquid temperature
T_{sat}	saturation temperature
T_{sub}	$=T_{sat}-T_L$; liquid subcooling temperature
T_{sup}	$=T_W-T_{sat}$; wall superheating
T_W	wall temperature
T_{LW}	liquid characteristic near-wall temperature
t_W	bubble waiting time
y^+	non-dimensional distance to the wall
U_G	vapour velocity
U_L	liquid velocity

Greek letters

ρ_G	density of the gaseous phase
ρ_L	density of the liquid phase
τ_W	wall shear stress

Subsripts

G	gaseous phase
L	liquid phase
in	inlet properties
max	maximum
ref	reference quantity
sub	subcooling
sup	superheating
tot	total

3. The Experimental Testcase

The present investigation of CFD model development and validation for nucleate subcooled boiling under almost normal pressure conditions has been based on a recently published series of experiments by Lee et al. (2008). Further experimental investigations on the same experimental test facility have been published in recent years (Lee et al., 2002 & 2009).

The test loop utilized in the cited experiments is aimed to the investigation of subcooled nucleate boiling in a vertical circular annulus with a centralized heater rod (see Fig. 1), where subcooled boiling occurs on the heated surface. The test section is a 2376mm long vertical concentric annulus with a heated inner tube. The inner tube is of R_0=9.5mm outer radius and electrically heated. The length of the heated test section is L_T=1670 mm consisting of an Inconel 625 tube with a 1.5 mm thickness. The tube is uniformly heated by a 54 kW DC power supply. The outer tube is comprised of two stainless steel tubes of R=18.75mm inner radius, which are connected, below the measuring plane, by a transparent glass tube of 50 mm length, therefore facilitating optical measurements of radial distributions of flow parameters. The circular annulus of the test section has a gap width of 9.25mm and therefore a hydraulic diameter of 18.5mm. The heated section begins at the same elevation as the test section inlet, and the measuring plane is located at L_M=1610mm downstream of the beginning of the heated section inlet.

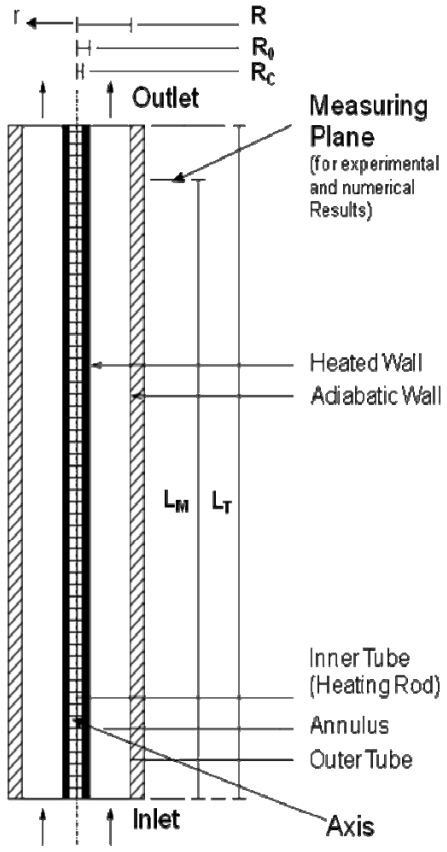

Figure 1: Schematic of the experimental test section of the vertical circular annulus in the experiments of Lee et al. (2008)

Experiments were carried out for the various levels of heat flux, mass flux, inlet liquid temperature and inlet pressure. A total of 32 data sets were investigated, where detailed measurement data for radial distributions of local void fraction, the vapour and the liquid velocities, Sauter mean vapour bubble diameter and the local interfacial area concentration are available for only 12 out of the 32 experimental conditions from (Lee et al., 2008). The local vapour phase parameters were measured by a double-sensor conductivity probe method traversed over 13 points in the measurement cross section of the annulus with the dimensionless width of the annulus:

$$R_P = \left(r - R_0\right) / \left(R - R_0\right) \quad (1)$$

between 0.11 and 0.90 to obtain the radial profiles of the local flow parameters. Here, r, R and R_0 are the radial location measured from the symmetry axis, inner radius of

outer tube and outer radius of inner tube, respectively. The local liquid velocity was measured by the Pitot tube method. Local bubble diameter and interfacial concentration has been reconstructed from these measured data in a post-processing step.

Set No.	q´´ [kW m^{-2}]	G [kg m^{-2}s]	T_{in} [°C]	P_{in} [kPa]
25	220.0	1057.2	90.1	134.4
16	320.4	718.8	83.8	121.1

Table 1: Investigated operating validation testcase conditions from the experiments of Lee et al. (2008)

Two distinct operating points of the experimental test facility, characterized by the applied wall heat flux q´´, the liquid mass flux at the test section inlet G, the inlet liquid temperature T_{in} and the inlet pressure level P_{in}, have been selected for CFD investigation. The data of these operating points are given in Table 1, where the data set numbers correspond to naming convention in the paper of Lee et al. (2008). Operating conditions had been selected such, that the Set25 represents the case, where the least of all vapor is produced, while Set16 represents the case with the largest amount of vapor.

4. The Physical Model

The flow under investigation is described in the framework of the currently most conventional CFD approach to modeling two-phase flows with significant volume fractions of both phases - the Eulerian two-fluid model derived under the assumption of interpenetrating continua. Material properties for both vapor and liquid had been specified by defining material properties based on IAPWS-IF97 water/water steam tables defined for the given range of temperature and pressure of the testcases. Phase distribution results from solving the phase-specific continuity equations for volume fractions, and separate sets of momentum equations are solved for each phase, where buoyancy and interfacial momentum transfer is taken into account. Momentum transport equations are supplemented by turbulence model equations, where the shear stress transport model (SST) has been applied to the continuous phase and a zero-equation disperse phase turbulence model together with the Sato bubble enhanced turbulence model have been used to describe the turbulence effects arising from the bubbly phase (for details see ANSYS Inc., 2009).

For the steam–water bubbly flow an energy equation is solved for liquid, while for the description of the nucleate subcooled boiling processes under consideration the vapour is assumed to be saturated at all time. The exchange of mass, momentum and heat between phases are modeled using the correspondent source terms in the phase-specific balance equations. For the dispersed bubbly flow assumed for the nucleate subcooled boiling processes the interfacial momentum transfer is modeled in terms of the Grace drag force due to the hydrodynamic resistance and the non-drag forces.

Regarding the consideration of the non-drag forces the current framework in ANSYS CFX (ANSYS Inc., 2009) allows for the inclusion of the lift, the wall lubrication, the virtual mass and the turbulent dispersion force. Further forces can be added by user-defined source terms. Previous investigations have shown good agreement for simulating adiabatic air-water bubbly flows (see Frank et al., 2008), polydispersed air-water and steam-water flows (see Krepper et al., 2008) as well as recondensing steam-water flows (see Lifante et al., 2009) using the formulations of Tomiyama (1995, 1998) for the lift force, the generalized wall lubrication force formulation by Frank (2005) and the Favre averaged drag turbulent dispersion force formulation by Burns et al. (2004). In the present investigation non-drag forces with the exclusion of the wall lubrication and virtual mass forces have been applied.

The modeling approach for wall boiling will be described in a separate section. Once the steam is produced at the wall, it will be assumed, that the steam is at local pressure dependent saturation temperature at all time. Further the steam condensates in the bulk subcooled liquid ($T_L < T_{sat}$) with the mass transfer rate per unit volume:

$$\dot{m} = \max\left(\frac{h_{LG}(T_{sat}-T_L)A_{LG}}{H_{LG}}, 0\right) \qquad (2)$$

With superheated liquid, fluid is evaporating at the rate:

$$\dot{m} = \max\left(\frac{h_{LG}(T_L-T_{sat})A_{LG}}{H_{LG}}, 0\right) \qquad (3)$$

A_{LG} is the interfacial area, and h_{LG} is the interfacial heat transfer coefficient, calculated according to Ranz and Marshall (1952):

$$h_{LG} = \frac{k_L}{d_B} Nu = \frac{k_L}{d_B}\left(2 + 0.6\,\mathrm{Re}^{1/2}\,\mathrm{Pr}^{1/3}\right) \qquad (4)$$

This relationship is valid for mass transfer at the interface of rather small bubbles with diameters well below 0.5mm. So recently Tomiyama (2009) proposed a slightly changed relationship for evaporation/condensation at the phase interface of larger bubbles in the range of d_B~1,…,3mm:

$$h_{LG} = \frac{k_L}{d_B} Nu = \frac{k_L}{d_B}\left(2 + 0.15\,\mathrm{Re}^{0.8}\,\mathrm{Pr}^{0.5}\right) \qquad (5)$$

To close the phase transition model in the bulk bubbly flow, a phasic characteristic length scale for the mean bubble diameter d_B has to be provided. This can be obtained from applying a population balance model like homogeneous/inhomogeneous MUSIG model or a DQMOM model. Here we follow the simplified approach of providing a local mean bubble diameter as proposed by Kurul and Podowski (1991) as well as Anglart et al. (1997), where both proposed to calculate the local bubble diameter d_B as a linear function of liquid subcooling T_{sub}:

$$d_B = \frac{d_{B1}\left(T_{sub}-T_{sub,2}\right) + d_{B2}\left(T_{sub,1}-T_{sub}\right)}{T_{sub,1}-T_{sub,2}} \qquad (6)$$

For typical nuclear energy applications these authors proposed for subcooled nucleate boiling under PWR conditions (so, high pressure conditions) reference bubble diameters at the two reference subcooling conditions: d_{B1} = 0.1mm at $T_{sub,1}$ = 13.5K and d_{B2} =2mm at $T_{sub,2}$ = -5K. The bubble size in the bulk has a direct influence on the interfacial area density and on the condensation respective evaporation rate in the bulk. It is clear, that these assumptions cannot be applied without reconsideration to the nucleate subcooled boiling under normal pressure

conditions, since already the experimental observations show, that Sauter mean bubble diameters of up to 4mm occurred in the experiments under some of the operating conditions. Therefore this relationship (5) was a first candidate for necessary model modifications for bulk and wall boiling under low pressure conditions, as will be discussed in a later section.

4.1. Modeling Nucleate Subcooled Boiling at Heated Walls

The current implementation and exposure of the wall boiling model in the graphical CFD preprocessor of ANSYS CFX 12.0 had predecessors in earlier versions of ANSYS CFX as beta model capabilities. Therefore more detailed descriptions of the wall boiling modeling approach exist from earlier publications, referring to Egorov et al. (2004) and Krepper et al. (2007). All this model development follow the general outline of the so-called wall heat flux partitioning algorithm developed by Kurul & Podowski (1991). Since this initial model development was aimed more on 1d thermohydraulic modeling of the phenomenon, model enhancements and adjustments were necessary in various places of the model algorithm formulation in order to accommodate for the specific requirements of an implementation into a general 3d CFD solver.

Subcooled boiling is observed at heated surfaces, when the heat flux applied to the wall is too high to be transferred to the core flow of liquid by the single-phase convective-conductive mechanisms. The term “subcooled” means, that the saturation temperature is exceeded only in a local vicinity of the wall, whereas the average temperature in the bulk is still below saturation.

The point, where the local wall temperature reaches the saturation temperature, is considered as the onset of nucleate boiling. Steam bubbles are generated at the heated surface at nucleation sites, with the surface density of these sites depending on different factors, including the wall superheat. With increasing wall superheat $\Delta T_{sup}=T_W-T_{sat}$ the attached bubbles grow and then leave the wall at certain critical size. This critical size, called bubble departure diameter, may depend on the surface tension and on the forces acting on the bubbles from the surrounding fluid.

Heat transfer from the wall is then described as being carried by turbulent convection of liquid, by transient conduction due to the departing bubbles and by evaporation. Distribution of the entire wall heat flux between these mechanisms (wall heat partitioning) can be calculated by modeling each mechanism in terms of the nucleation site density, the size of departing bubbles, their detachment frequency, and waiting time until the next bubble appears on the same site (mechanistic modeling approach). This mechanistic modeling approach of the wall boiling process is required in the framework of the CFD code, since for technical applications it is mostly impossible to fully resolve the micro-phenomenon of steam bubble formation at the heated wall on the underlying numerical mesh and with the applied time scale of integration. Instead the resulting steam production and enhanced heat transfer to the liquid is taken into account by the mechanistic model of wall boiling based on the wall heat flux partitioning algorithm. Once the steam bubbles are released from the nucleation sites, they move through the subcooled liquid and condensate, releasing the latent heat again in correspondence to eq. (1).

Following the modeling approach of wall heat flux partitioning, the applied wall heat flux on the heated surface is split into 3 parts: Q_C, the turbulent convective heating of the liquid, Q_Q, the quenching heat flux and Q_E, the evaporative heat flux:

$$Q_W = Q_C + Q_Q + Q_E \tag{7}$$

As already mentioned, in this model vapour is assumed to be saturated everywhere, and no part of the wall heat flux is arranged for superheating of the vapour phase. The heat partitioning model considers the whole heated wall surface as being separated into two fractions: a) fraction A_2 influenced by the vapour bubbles, formed on the wall and b) fraction A_1 being the remaining wall surface area with $A_1=1-A_2$. The wall area fraction A1 represents the part of the wall surface that is not affected by the growing steam bubbles. Therefore the wall heat flux for this part of the surface is modelled in a similar way as for the single-phase convective heat transfer into pure liquid, by using the turbulent wall function procedure as outlined in Egorov et al. (2004). Given that, the convective heat flux can be written as:

$$Q_C = A_1 h_C \left(T_W - T_L\right) \tag{8}$$

where h_C is the turbulent heat transfer coefficient, which depends on the velocity field and is modelled using the turbulent temperature wall function (see Egorov et al., 2004). The wall area fraction A_2 represents the remaining part of the surface, which exchanges heat with both phases. The already mentioned evaporative heat flux Q_E is consumed for evaporation of the initially subcooled liquid:

$$Q_E = \dot{m}\left(h_{G,sat} - h_L\right) \tag{9}$$

with:

$$\begin{aligned}\dot{m} &= \rho_G \frac{\pi d_W^3}{6} N_a f \\ &= \rho_G A'_{2F} \frac{2}{3} d_W f \\ &= \rho_G \min\left(\frac{\pi a^2 d_w^2}{4}, 5\right)\frac{2}{3} d_w N_a f\end{aligned} \tag{10}$$

resulting in:

$$Q_E = \frac{2}{3}\rho_G d_W \min\left(\frac{\pi a^2 d_w^2}{4}, 5\right) N_a f\, h_{LG} \tag{11}$$

where $\dot{m}$ is the evaporation mass transfer rate per unit wall area, A'_{2F} is the non-limited wall area influenced by vapour bubble formation, $h_{G,sat}$ and h_L are the specific enthalpies of the saturated vapour and subcooled liquid respectively, d_W is the bubble departure diameter, N_a is the nucleation site density and f is the bubble detachment frequency. The quenching heat flux due to transient vapour bubble departure and cooling of the wall area A_2 by substituting fresh subcooled liquid is modelled as:

$$Q_Q = A_2 h_Q \left(T_W - T_L\right) \tag{12}$$

where h_Q is the quenching heat transfer coefficient. In the above relationships the area A_2 influenced by the growing vapour bubbles is related to the nucleation site density and the bubble departure diameter:

$$A_2 = \min(\pi \frac{a^2 d_W^2}{4} \cdot N_a, 1) \quad (13)$$

where d_W is the bubble departure diameter, N_a is the nucleation site density and a is a influence factor introduced by Kurul & Podowski (1991) and is assumed to be a=2.
In order to arrive at a closed model formulation for the above wall heat flux partitioning scheme, a larger number of closure models have to be provided. These are required for the following model parameters:

- N_a, wall nucleation site density
- b_W, bubble departure diameter
- f, bubble detachment frequency
- h_Q, quenching heat transfer coefficient
- bubble waiting time

The required closure relationships are provided from correlations, following in most cases the used correlations in the original model formulation of Kurul & Podowski (1991), but providing alternatives or the possibility for the model user to introduce his own model correlation as a user-defined relationship instead. For more details on the different submodels please refer to (ANSYS Inc., 2009).
One particular and rather important correlation used in this model closure is introduced for the bubble departure diameter. Here Kurul & Podowski (1991) adopted a correlation established by Tolubinski & Kostanchuk (1970):

$$d_W = \min\left(d_{ref} \cdot \exp\left(-\frac{\Delta T_{sub}}{\Delta T_{ref}} \right), d_{\max} \right) \quad (14)$$

The parameters of the original model are dimensional (d_{max}=1.4mm, d_{ref}=0.6mm, ΔT_{ref}=45K) and ΔT_{sub} refers to the local liquid subcooling. These model data are specific for the model application to nucleate subcooled boiling under pressurized conditions and need to be revised in case of model application to different operating conditions.

4.2. Boundary Conditions for the Wall Boiling Model

The implementation of the wall boiling model for nucleate subcooled boiling in ANSYS CFX 12.0 supports the specification of either a prescribed wall heat flux or a prescribed wall temperature at the surface of the heated wall. Eq. (6) provides in both cases the relationship to predict either the resulting wall temperature in dependence on the prescribed wall heat flux or vice versa.
Another, and in practical cases even more interesting possibility, is the specification of a volumetric energy source in the solid material of the heater and the prediction of the heat transfer due to conduction in the solid material using conjugate heat transfer (CHT) prediction. In this case both the wall heat flux and the wall temperature are part of the solution from a coupled simulation of CHT in the solid material and multiphase flow CFD in the fluid domain of the application. ANSYS CFX 12.0 supports this type of simulation with both 1:1 and non-conforming meshes at the fluid-solid interface.

5. Model Validation based on CFD Simulation of the Testcase of Lee et al. (2008)

Formerly the wall boiling model, described in the previous section, was already thoroughly validated (e.g. Krepper et al., 2007) for nucleate subcooled boiling under pressurized conditions using the data from vertical channel or pipe experiments with heated outer walls for comparison, e.g. experiments published by Bartolomej and Chanturiya (1967) and Bartolomej et al. (1982).
In the present investigation the wall boiling model is applied to non-pressurized conditions, using the testcase configuration from the experimental test facility and experimental data of Lee et al. (2008), as described in section 3. To identify the range of validity of applied boiling model and undertaken model parameter changes the calculated steam volume fraction and steam/water velocity profiles were compared with the large set of measurements at different operating conditions.

5.1. CFD Simulations with Prescribed Wall Heat Flux

5.1.1. CFD Geometry and Numerical Meshes

Due to the radial symmetry of the circular annulus of the experimental test facility of Lee et al. (2008) the CFD simulations have been carried out two-dimensional on a 1 degree symmetry sector of the geometry. A hierarchy of consistently refined hexahedral meshes have been generated. In all cases the meshes had 1 mesh cell in circumferential direction and mesh nodes in radial and axial direction of the circular annulus were uniformly distributed. Main meshing parameters are listed in Table 2, where the dimensionless wall distance y^+ is evaluated at the heater wall of the configuration.

	Grid 1	**Grid 2**	**Grid 3**
No. of nodes	6.342	24.682	97.362
No. of elements	20×150	40×300	80×600
y^+ (Set25)	88	45	25
Max. aspect ratio	~24	~24	~24
Max. cell volume ratio	~1.01	~1.01	~1.01

Table 2: Mesh hierarchy for the CFD investigation.

5.1.2. Boundary conditions

Fig. 2 shows the schematic of the 1 degree slice of the circular annulus representing the fluid domain for the CFD simulation of the testcases of Lee et al. (2008). As shown, symmetry boundary conditions are applied to both sides of the symmetry segment, the outer wall of the circular annulus was set to adiabatic and a constant wall heat flux boundary condition has been applied to the surface of the centralized heater rod.
For the inlet boundary conditions it was assumed, that the test section of Lee et al. allows for fully developed turbulent inflow conditions. In order to account for that, single phase isothermal water flow at specified pressure, temperature and mass flow rate through the same 1670mm long test section was previously calculated, applying the SST turbulence model. The boiling flow simulation was afterwards initialized with the profile data of all velocity components, turbulent kinetic energy and turbulent eddy dissipation from the outlet cross section of this predecessor single-phase flow calculation. The same data where prescribed as inlet

boundary conditions of the liquid phase for the boiling flow simulation. For the steam phase a very small volume fraction of 10^{-15} and the saturation temperature corresponding to the prescribed pressure level including hydrostatic pressure in the circular annulus of the Lee et al. testcase geometry was prescribed at the inlet cross section. The reference pressure of the individual calculations was set to the corresponding pressure as specified by Lee et al. for the individual datasets and an average static pressure outlet boundary condition was applied.

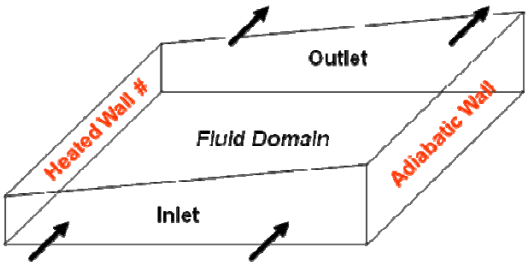

Figure 2: Geometry configuration and boundary conditions of CFD simulations with prescribed wall heat flux.

5.1.3. Wall Boiling Submodels and Parameter Modifications

As already mentioned, the wall boiling model depends on a larger number of submodels and model parameters, where most of them had been derived for wall boiling processes under pressurized conditions. In the present investigation the following settings for the submodels of the wall boiling model have been used:

- Wall nucleation site density: Lemmert & Chawla model
- Liquid quenching heat transfer coefficient: Del Valle Kenning model
- Bubble detachment frequency: Cole model, derived from terminal bubble rise velocity over the bubble departure diameter
- Bubble waiting time: Tolubinski & Kostanchuk model, which sets the bubble waiting time to 80% of the time between bubble departures
- Bubble diameter influence factor: default value of 2.0
- Fixed y^+ for evaluation of liquid subcooling temperature from turbulent wall functions: default value of 250

For details of the named submodels please refer to ANSYS Inc. (2009). Special attention has been directed to the modelling of the bubble diameter in the bulk liquid d_B, the bubble departure diameter d_W and the maximum area fraction of bubble influence $A_{2,max}$.

The default for the modelling of the bubble diameter in the bulk liquid under pressurized conditions is the relationship introduced by Kurul & Podowski (1991) in accordance with eq. (5), relating the bubble diameter in the bulk liquid in a piece-wise linear relationship to the local liquid subcooling temperature with default model parameters resulting in a maximum bubble diameter of $d_B \leq 1.48$mm (see Fig. 4). From the experimental data from Lee et al. (2008) it can be seen, that e.g. under the experimental conditions of the dataset Set25 maximum bubble diameters of about $d_{B,max}=2.8$mm have been measured. Under different operating conditions even larger bubble diameters of up to $d_{B,max}\sim 4.2$mm have occurred in the experiments under normal pressure conditions. Partially the large bubble diameters in the bulk liquid can result from bubble coalescence due to the higher steam volume fraction in the vicinity of the heater wall. Unfortunately without applying a population balance model in combination with the wall boiling model we cannot account for these bubble coalescence effects. Instead it was tried to take into account the larger observed bubble diameters, which are especially of importance for the rate of steam recondensation in the subcooled liquid, carrying out a parameter study with the settings from Table 3. Following a suggestion of Egorov et al. (2004), the original piece-wise linear relationship of Kurul & Podowski (1991) was additionally smoothed by applying *tanh* functions as smoothing function. The resulting bubble diameters in the bulk liquid in dependence on the local liquid subcooling can be seen in Fig. 4 for the original Kurul & Podowski law and the made modification 3.

Modification	d_{B1}	$T_{sub,1}$	d_{B2}	$T_{sub,2}$
Kurul & Podowski (1991)	0.1mm	13.5K	2.0mm	-5K
d_B, Mod. 1	0.15mm	13.5K	4.0mm	-5K
d_B, Mod. 2	0.15mm	13.5K	4.0mm	5K
d_B, Mod. 3	0.15mm	25.0K	4.0mm	5K

Table 3: Parameter modifications regarding the modeling of the bubble diameter in the bulk liquid.

Modification	d_W
Tolubinski & Kostanchuk (1970)	from eq. (13)
d_W, Mod. 1	d_W=1mm
d_W, Mod. 2	d_W=2mm
d_W, Mod. 3	d_W=3mm
d_W, Mod. 4	from eq. (13) multiplied by 4.0

Table 4: Parameter modifications regarding the modelling of the bubble departure diameter.

A direct consequence of the modifications made for the modelling of the bulk bubble diameter is a resulting change of the bubble departure diameter, since both bubble diameter laws should give consistent values close to the surface of the heater. Furthermore it is even more important, that the bubble departure diameter is of main influence on the area of bubble influence on the heated wall, bubble departure frequency and thereby finally on the evaporation rate and steam production resulting from the wall boiling model. For the given operating conditions of Set25 the standard relationship of Tolubinski & Kostanchuk (1970) results in a bubble departure diameter of about 0.5mm, which seems to be much too small in comparison to the near wall bubble diameter measurements. Therefore a parametric study has been carried out for the bubble departure diameter d_W with the different model settings as listed in Table 4.

Finally, in a number of previous investigations the wall area influenced by the vapour bubbles A_2 was limited by a maximum area fraction of bubble influence $A_{2,max}=0.5$ by default. However it was found, that for the present testcase with the increased bubble departure diameters this artificial

limitation of A_2 results in a rather early limitation of the evaporative heat flux and thereby the amount of produced steam volume fraction from the wall boiling model was substantially underpredicted in comparison to the experiments. Therefore this limitation was raised by setting $A_{2,max}$=1.0 throughout the carried out CFD simulations.

5.1.4. Results and Comparison to Experimental Data

First CFD investigations based on the specification of the Set25 dataset from the Lee et al. (2008) experiments were related to investigation of numerical parameters and the adherence to CFD best practice guidelines. Simulations had been carried out in steady-state, applying the ANSYS CFX high-resolution scheme (2nd order TVD scheme) as advection scheme for the hydrodynamic system of equations and 1st order upwind scheme for the turbulence model equations. For convergence control a RMS residual criteria of 10^{-4} has been applied. Additionally global mass, momentum and energy as well as temperature and volume fraction data in 60 axially and radially distributed monitoring point locations have been monitored and were found to finally result in stationary values. Furthermore it was investigated and found, that the steady-state solution algorithm requires for the desired level of convergence integration time scales in the range of Δt~0.2,…,100ms, which is case and mesh resolution dependent. For the mesh level 3 and Set25 operating conditions an integration time scale of 0.4ms was required.
In a first series of CFD simulations the influence of the parametric change for the bubble diameter in the bulk liquid has been investigated. Fig. 5 shows the resulting radial distributions for the vapour volume fraction and bubble diameter at the measurement location in comparison to the data of Set25 (the local bubble diameter being a direct result from the Kurul & Podowski law in accordance to eq. (3) and the local liquid subcooling temperature $T_{sub}=T_{sat}-T_L$). It can be seen from Fig. 5a), that the changes in the modelling parameters for the 3 modifications of the bulk bubble diameter have led to a decrease in the maximum value of the steam volume fraction directly at the heater surface and to an increase in the steam volume fraction further apart from the heated wall. The slope of the steam volume fraction profiles are in better agreement with the experimental data for higher bulk bubble diameters closer to the experimentally measured values, as can be expected. Nevertheless the total amount of produced steam is still underpredicted and it can be seen from the last 2 modifications that a further increase in bubble bulk diameter seems not to have a further influence. With the 3rd modification of the bulk bubble diameter the results for the predicted bubble diameters are now in the same order as the measured values (see Fig. 5b).
Setting d_B=2mm and $A_{2,max}$=1.0 a second series of parameter investigation has been carried out for Set25 operating conditions. Fig. 6 a)-c) show the CFD-experiment comparison of profiles of vapour volume fraction, axial water and vapour velocities at the measurement cross section. With the 3rd modification of the bubble departure bubble diameter in accordance to Table 4 and Fig. 4 a reasonable good agreement between the numerically predicted and measured vapour volume fraction profiles could be established (Fig. 6a). Water velocities are in good agreement to measured data in a certain distance from the heated wall (Fig. 6b). But close to the heated wall the water velocities from the CFD simulation clearly show an axial acceleration due to buoyancy and the applied free slip wall boundary condition of the vapour phase, resulting in a larger difference to the measured water velocities. A corresponding difference between predicted and measured vapour velocities can be observed from Fig. 6c) in the vicinity of the wall, while the comparison to data in a certain distance from the wall is quite satisfactory. An explanation of the observed differences is, that in the reality of a wall boiling process on a vertical heated surface the steam bubbles initially grow on the heated surface without moving. Later a sliding motion of the growing steam bubbles has been observed in experiments for bubble diameters close to the departure diameter and if the buoyancy force on the growing steam bubble becomes large enough. Nevertheless the sliding velocity of these steam bubbles is substantially slower than the rising velocity of steam bubbles in free stream motion, which can explain the observed differences in vapour velocity. A changed wall boundary condition based on an estimated bubble sliding velocity could contribute to improvement of this comparison. On the other hand side some doubt regarding the measured vapour velocities is remaining, where no buoyancy effect from the approx. 30% vapour volume fraction close to the wall is remarkable in the data.
Finally Fig. 7 shows the result of a grid convergence study, where the final model parameter settings for Set25 have been applied to the series of even 4 subsequently refined meshes. The radial volume fraction profiles show a tendency to a slight further increase in the predicted vapour volume fractions, also the difference between mesh 3 and 4 becomes rather small and is in fair agreement to the experimental data from lee et al. (2008).

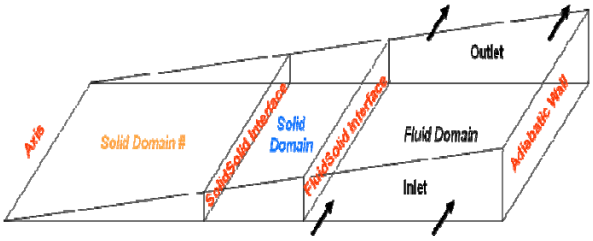

Figure 3: Geometry configuration and boundary conditions of CFD simulations with prescribed volumetric energy source in the solid core material of the heating rod.

5.2. CFD Simulations with Prescribed Volumetric Energy Source in the Solid Core Material of the Heating Rod

An alternative to the specification of the wall heat flux or a given wall temperature is the specification of a volumetric energy source in the solid material of the heater. In fact in many cases this is the more desirable simulation approach, since e.g. the thermal energy output of the heater is known whereas the wall temperature and the wall heat flux are rather sought as part of the solution. In ANSYS CFX 12.0 the prediction of conjugate heat transfer (CHT) in solid materials has been interfaced with the heat partitioning algorithm of the wall boiling model. The combination of

both physical models is supported on fluid-solid interfaces with 1:1 and non-conforming meshes (GGI – General Grid Interface).

5.2.1. Numerical Meshes and Boundary Conditions

In order to demonstrate the capability of ANSYS CFX 12.0 to combine CHT and wall boiling model, a corresponding setup for the heating rod with a volumetric energy source term has been set up. For the operating conditions of the dataset Set25 the prescribed wall heat flux of q´´=220 kW m^{-2} corresponds to a volumetric energy source of E=82.3 MW m^{-3}. Hereby the volumetric energy source has been specified in an inner core of the solid material of the heating rod with a radius R_{Core}=0.75 R_0=7.125mm, as can be seen from Fig. 3. The outer non-heated cladding has been specified in this case as 0.75 $R_0 \leq R_{Cladding} \leq R_0$., introducing thereby a solid-solid interface between the homogeneously heated core and the non-heated cladding material and a fluid-solid interface between the cladding and the fluid domain, where the wall boiling will occur. Both core and cladding solid materials have been set to steel properties. Symmetry boundary conditions apply to the boundary patches in circumferential direction (front and rear), the top boundaries of the core and cladding domains have been set to adiabatic, while for the bottom boundaries of both solid domains an isothermal boundary condition with the fluid inlet temperature of the dataset under consideration has been applied.
Investigations and comparisons to existing CFD solutions from section 5.1 and the experimental data have been carried out on all 3 mesh levels using conforming meshes and on mesh level 3 only for non-conforming mesh interfaces. In this case the following fluid-solid domain meshing combinations have been investigated:

Configuration 1 (mesh levels 1-3):
- Fluid domain – mesh from Table 2;
- Core & Cladding solid – hexahedral meshes with same mesh resolution as the fluid domain;
- all mesh interfaces are treated as 1÷1 conforming meshes with direct data transfer

Configuration 2:
- same mesh as grid level 3 of Configuration 1;
- all mesh interfaces are treated as GGI interfaces[1]

Configuration 3:
- Fluid domain – 80x603 cell hexahedral mesh;
- Core solid – 80x600 cell hexahedral mesh;
- Cladding solid – 80x600 cell hexahedral mesh;
- all mesh interfaces are treated as GGI interfaces

5.2.2. Results and Comparison to Experimental Data

Fig. 8 shows the resulting solid/fluid temperature and steam volume fraction distribution in the vertical plane for the CFD simulation with a prescribed volumetric energy source in the heated core of the heater rod. From the left hand side image it can be seen, that the temperature distribution in the solid material is quite homogeneous over the height of the heating rod, while in the fluid domain the fluid temperature is continuously increasing from the inlet to the outlet cross section. The latter corresponds to a continuously increasing amount of steam being produced at the heated surface of the heater rod (right image).
For the measurement cross section at L_M=1610mm the solid and fluid temperatures have been compared for Configuration 1 on three consistently refined meshes (see Fig. 9). From this figure it can be seen, that the resulting solid temperatures are almost identical on all 3 meshes, while the fluid temperatures slightly differ. Additionally in the fluid domain the fluid temperatures are compared to the CFD result from the simulation with the prescribed constant wall heat flux, where only a rather minor difference in the results could be observed. Fig. 10 shows the same comparison for results on 3 different meshes of Configuration 1 for the radial steam volume fraction distribution at the measurement cross section with the additional comparison to experimental data. Here the resulting steam volume fraction on mesh level 3 for the CHT Configuration 1 leads to even a slightly higher steam volume fraction in a certain distance from the wall, what corresponds well to the slightly higher liquid temperatures from Fig. 9 (and therefore a slightly lower steam recondensation rate at this radial location).
Finally CFD results from the 3 different meshing configurations defined in section 5.2.1 using two different approaches for the data transfer between meshes on both sides of a meshing interface (1÷1 direct data exchange and GGI) have been compared to each other in Fig.11a)-b). The diagrams in Fig. 11 show that identical results for radial temperature and steam volume fraction distributions are obtained with all three meshing & data exchange methods, proofing the correctness of the corresponding algorithmic implementations for the combination of CHT and the wall boiling model in ANSYS CFX 12.1.

Conclusions

A wall boiling model for the CFD prediction of nucleate subcooled boiling has been implemented in ANSYS CFX 12.0 together with the necessary underlying submodels for model closure and GUI support in the ANSYS CFX physical preprocessor. In earlier publications (see Egorov et al. (2004), Krepper et al. (2007, 2008)) the model had been successfully validated for nucleate subcooled boiling under pressurized conditions. In the present work, the model has been applied to the validation experiment of Lee et al. (2008), which is aimed to nucleate subcooled boiling under normal pressure conditions in flow geometry with dimensions very similar to the arrangement of heated rods, which can be found in nuclear reactor fuel assemblies. In this paper the model parameters have been identified, which have to be changed for a successful CFD prediction of wall boiling and steam production under the operating conditions of the selected testcase. Special model modification with regard to the prediction of the local liquid subcooling temperature in the nearest wall mesh cell lead to a stabilization of the model and thereby to almost grid independent results of the CFD prediction of the wall boiling process. The comparison to the experimental data of Lee et al. (2008) led to satisfactory agreement, taking into account the measurement accuracy in the experiments and the remaining uncertainties in the correlations used in wall boiling model closure.
Furthermore the wall boiling heat partitioning algorithm has

[1] GGI – General Grid Interface

been coupled to the prediction of conjugate heat transfer (CHT) in the solid material of the heated boundary of the fluid domain, allowing for the definition of volumetric energy sources in e.g. the rods of nuclear fuel assemblies heated by nuclear fission reaction instead of fluid domain thermal boundary conditions. The model implementation supports both conforming and non-conforming meshes at domain interfaces. In the validation exercise it has been proven that the different meshing and data exchange approaches lead to identical results of the CFD simulation.

Acknowledgements

This research has been supported by the German Ministry of Economy (BMWi) under contract number 150 1328 in the framework of the German CFD Network on Nuclear Reactor Safety Research and Alliance for Competence in Nuclear Technology, Germany.

References

Anglart, H., Nylund, O., Kurul, N., Podowski, M.Z.: “CFD prediction of flow and phase distribution in fuel assemblies with spacers”, NURETH-7, Saratoga Springs, New York, 1995. Nuclear Eng. & Design (NED), Vol. 177 (1997), pp. 215–228.

ANSYS Inc., ANSYS CFX 12.0: Users Manual, 2009

Bartolomej, G.G., Chanturiya,V.M.: “Experimental study of true void fraction when boiling subcooled water in vertical tubes”, Thermal Engineering, Vol. 14 (1967), pp. 123–128 (translated from Teploenergetika, no. 2, Vol. 14 (1967), pp. 80–83).

Bartolomej, G.G., et al.: „An experimental investigation of true volumetric vapour content with subcooled boiling in tubes”, Thermal Engineering, Vol. 29 (1982), pp. 132–135 (translated from Teploenergetika, no. 3, vol. 29, 1982, pp.20–23).

Burns A.D., Frank Th., Hamill I., Shi J.-M.: "The Favre Averaged Drag Model for Turbulent Dispersion in Eulerian Multi-Phase Flows", 5th International Conference on Multiphase Flows, ICMF'2004, Yokohama, Japan, May 31 - June 3, 2004, paper No. 392, pp. 1-17.

Egorov, Y., Menter, F.: “Experimental Implementation of the RPI Wall Boiling Model in CFX-5.6”, Technical Report ANSYS/TR-04-10, ANSYS Germany GmbH (2004).

Frank Th.: "Progress in the numerical simulation (CFD) of 3-dimensional gas-liquid multiphase flows", 2. NAFEMS CFD-Seminar "Simulation komplexer Strömungsvorgänge (CFD) - Anwendungen und Entwicklungstendenzen", Wiesbaden, Germany, 25.-26. April 2005, pp. 1-18.

Frank Th., Zwart P.J., Krepper E., Prasser H.-M., Lucas D.: "Validation of CFD models for mono- and polydisperse air-water two-phase flows in pipes", J. Nuclear Engineering & Design (NED), Vol. 238, pp. 647-659, March 2008.

Krepper E., Koncar B., Egorov Y.: “CFD modeling of subcooled boiling - Concept, validation and application to fuel assembly design", Nuclear Engineering and Design (NED), Vol. 237, pp. 716-731, 2007.

Krepper E., Lucas D., Frank Th., Prasser H.-M., Zwart P.J.: "The inhomogeneous MUSIG model for the simulation of polydispersed flows", Nuclear Engineering and Design (NED), Vol. 238, pp. 1690-1702, 2008.

Kurul N., Podowski M.Z., On the Modelling of Multidimensional Effects in Boiling Channels, ANS Proc. 27th National Heat Transfer Conference, Minneapolis, July 28- 31, 1991.

Lee T.-H., Park G.C., Lee D.J.: „Local flow characteristics of subcooled boiling flow in a vertical concentric annulus“, International J. Multiphase Flows, Vol. 28 (2002), pp. 1351-1386.

Lee T.-H., Yun B.-J., Park G.-C., Hibiki T., Kim S.-O.: “Local flow structure of subcooled boiling flow of water in a heated annulus”, Proceedings of the 16th International Conference on Nuclear Engineering (ICONE-16), May 11-15, 2008, Orlando, Florida, USA, Paper No. ICONE16-48170, pp. 12.

Lee T.-H., Situ R., Hibiki T., Park H.-S., Ishii M., Mori M.: “Axial developments of interfacial area and void concentration profiles in subcooled boiling flow of water”, Int. J. Heat and Mass Transfer, Vol. 52 (2009), pp. 473-487.

Lifante C., Frank Th., Burns A.D.: "Prediction of Poly-disperse Steam Bubble Condensation in Subcooled Water using the Inhomogeneous MUSIG Model", ANSYS Conference & 27. CADFEM Users Meeting, Congress Center Leipzig (CCL), 18.-20. November 2009, pp. 1-30.

Ranz, W.E., Marshall, W.R.: “Evaporation from drops”, Chem. Eng. Progr., Vol. 48 (3), pp. 141–146 (1952).

Tolubinsky, V.I., Kostanchuk, D.M.: “Vapor bubbles growth rate and heat transfer intensity at subcooled water boiling”, Heat Transfer, Preprints of papers presented at the 4th International Heat Transfer Conference, Vol. 5, Paris (Paper No. B-2.8), 1970.

Tomiyama A., Sou A., Zun I., Kanami N., Sakaguchi T.: “Effect of Eotvos number and dimensionless liquid volumetric flux on lateral motion of a bubble in a laminar duct flow”, Advances in Multiphase Flow, p. 3-5, Elsevier Science (1995).

Tomiyama A.: “Struggle with computational bubble dynamics”, ICMF’98, 3rd Int. Conf. Multiphase Flow (ICMF), Lyon, France, 1998.

Tomiyama A.: Private communication (2009).

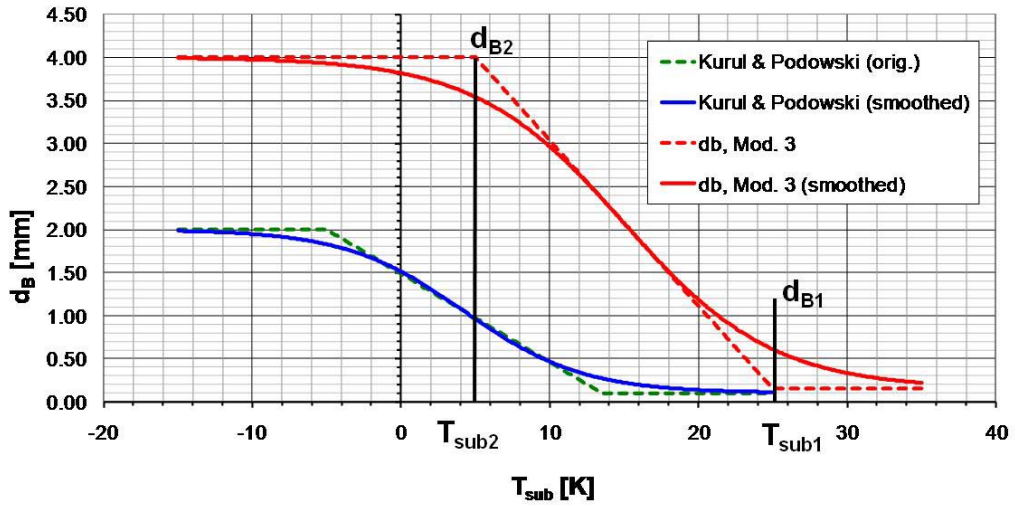

Figure 4: Bubble diameter in the bulk fluid in dependence on the local liquid subcooling temperature: Kurul & Podowski (1991) vs. 3rd modification of the bubble bulk diameter relationship.

a)

b)

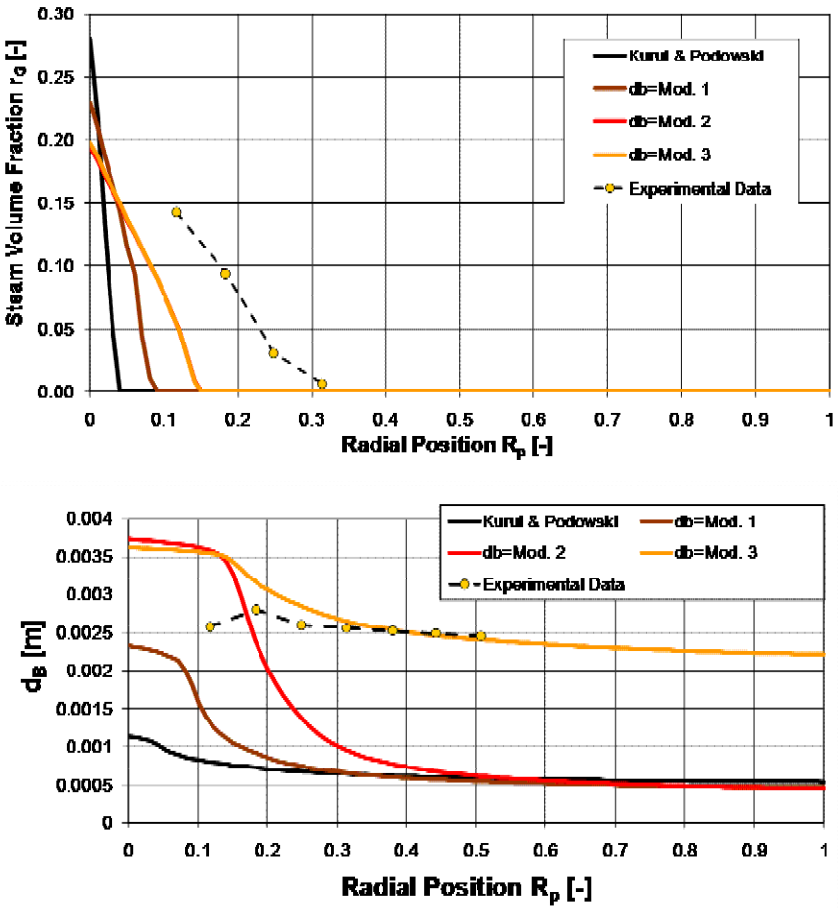

Figure 5: a) Steam volume fraction and b) bubble bulk diameter radial profiles for Set25 operating conditions on mesh level 3 for the different parameter variations in the bubble bulk diameter dependence on local liquid subcooling temperature.

a)

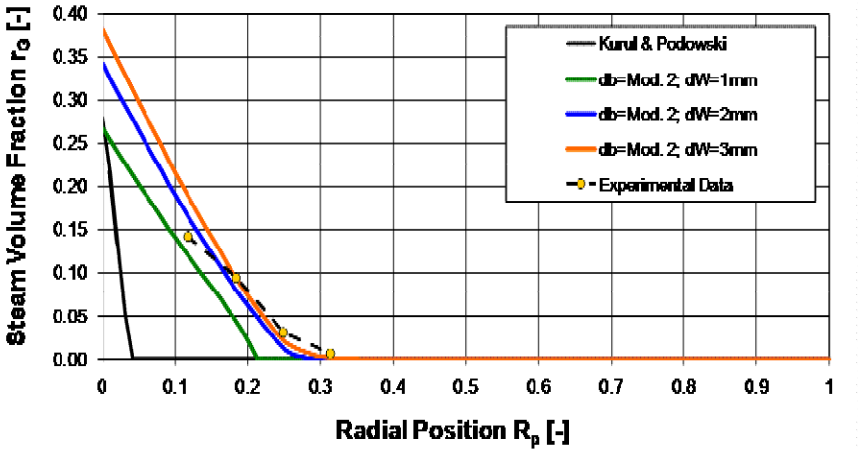

b)

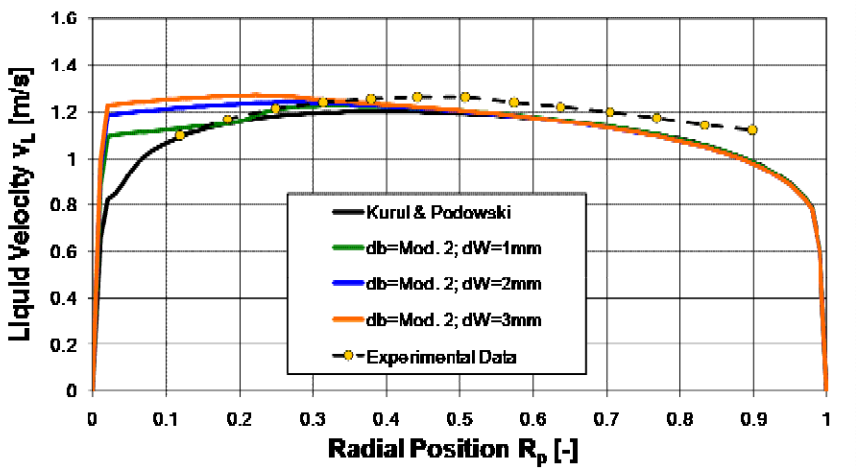

c)

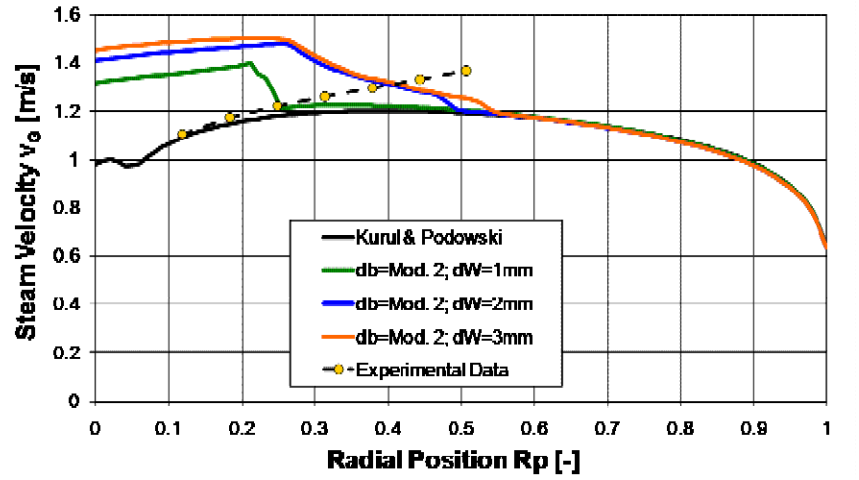

Figure 6: a) Steam volume fraction, b) water axial velocity and c) steam axial velocity radial profiles at measurement location for Set25 operating conditions on mesh level 3 for the different parameter variations in the bubble bulk diameter d_B and bubble departure diameter d_W.

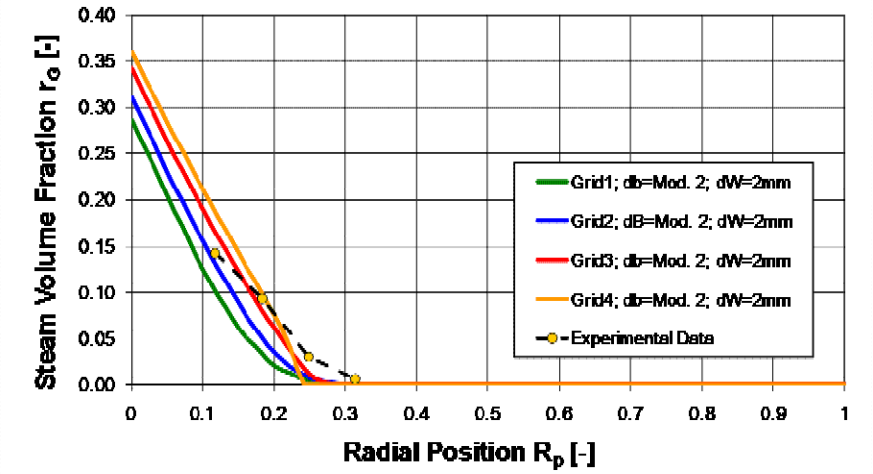

Figure 7: Investigation of grid independence of solution for steam volume fraction at measurement location for Set25 testcase and given model parameter changes for bubble bulk diameter and bubble departure diameter.

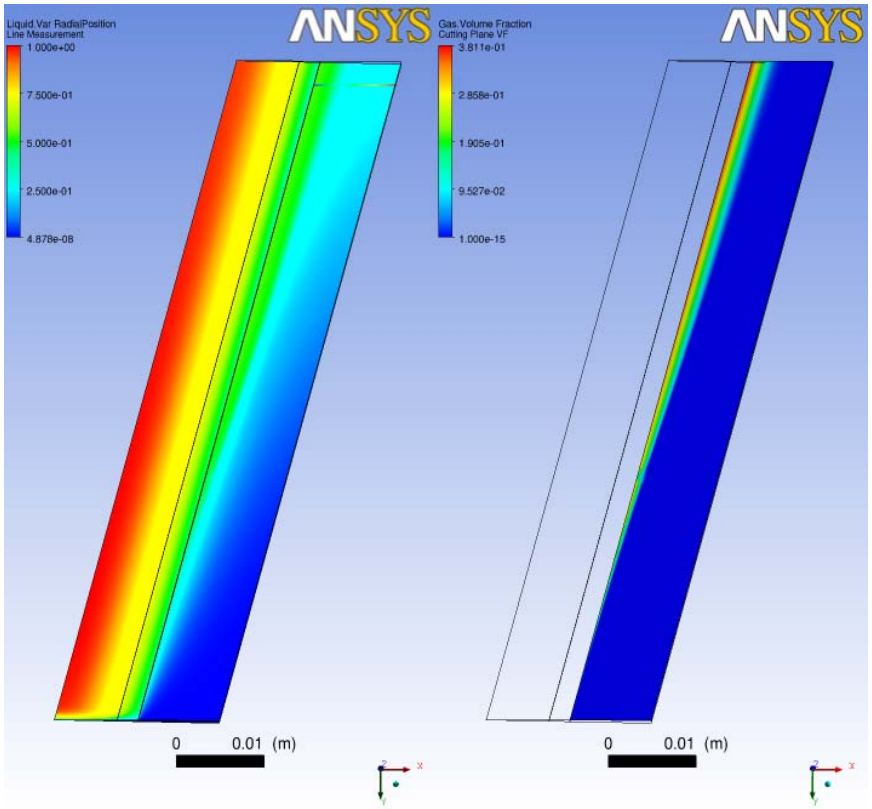

Figure 8: Solid/fluid temperature (left) and steam volume fraction (right) distribution in a vertical cross section of the heating rod and circular annulus of the Lee et al. testcase configuration.

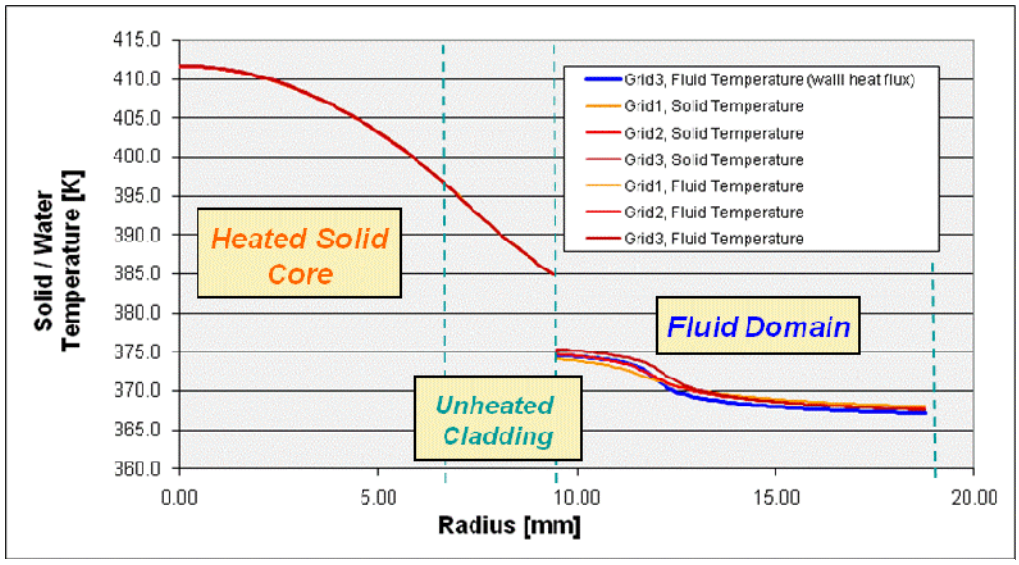

Figure 9: Comparison of temperature distributions in the solid materials of the heated core, the cladding material and water temperatures in the adjacent fluid domain at the measurement cross section of the Lee et al. testcase, Set25. Comparison to CFD results from simulation with specified wall heat flux at the heated wall (blue line).

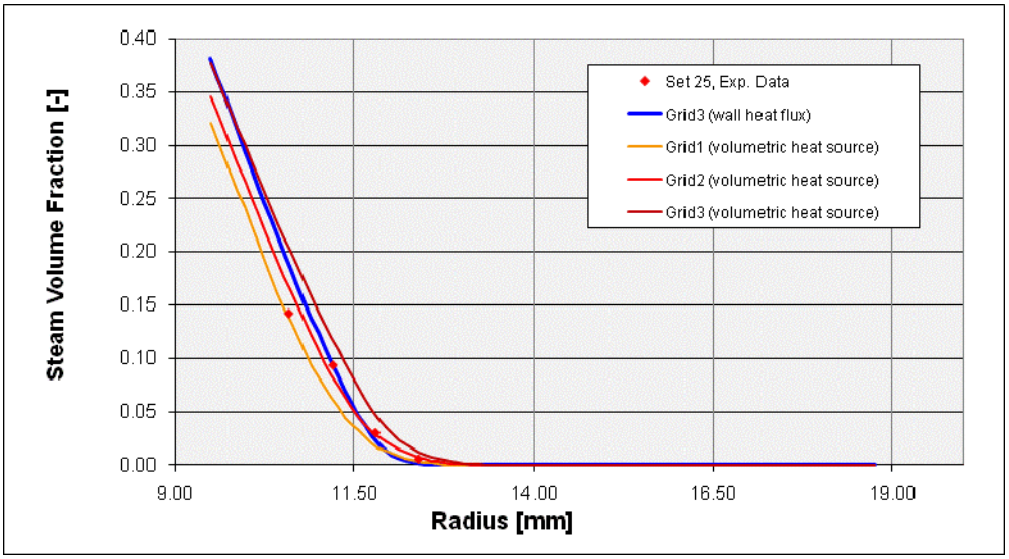

Figure 10: Comparison of experimental data for radial steam volume fraction distribution to CFD results for the Lee et al. testcase under Set25 operating conditions with specified wall heat flux at the heated wall and with specified volumetric energy source in the solid material of the heater.

a)

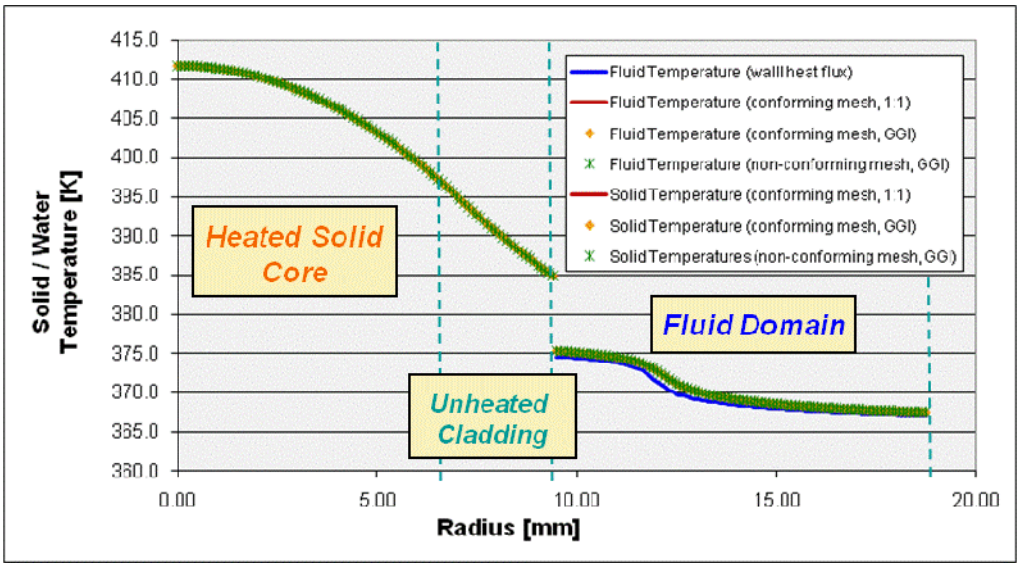

b)

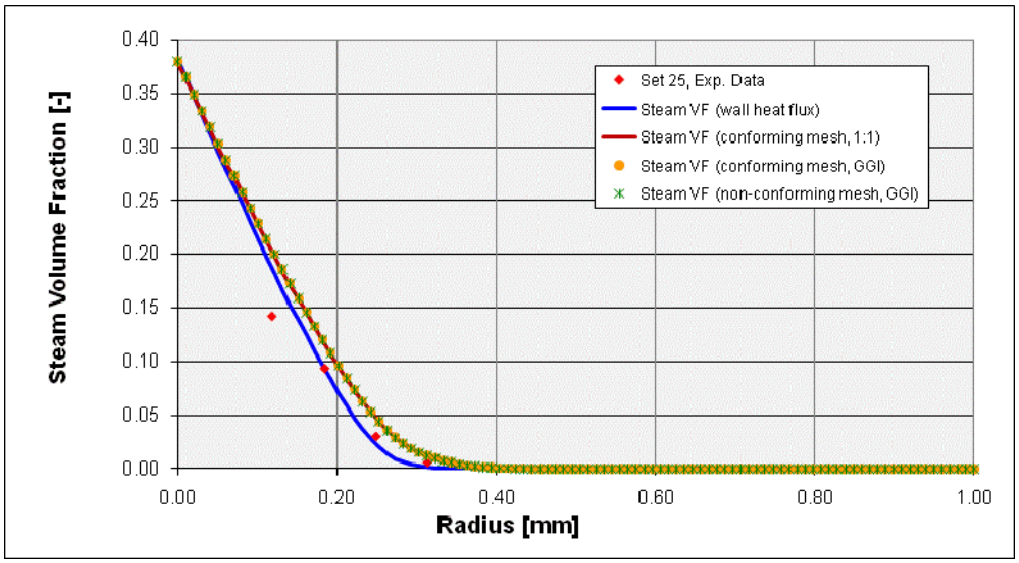

Figure 11: Comparison of a) radial temperature distributions in the solid materials of the heated core, the cladding material and water temperatures in the adjacent fluid domain and b) radial steam volume fraction distribution at measurement location for the three different configurations of conforming and non-conforming meshes with 1÷1 and GGI data connection at the meshing interfaces of adjacent domains.